Supporting Information

Prudhomme et al. 10.1073/pnas.1222473110

Precipitation Changes

The different global climate models (GCMs) used in our multimodel ensemble (MME) experiment show a range of precipitation patterns (Fig. S1), which will contribute to the spatial distribution of the MME results.

Global Impact Models

Global impact models (GIMs) vary in the types of processes represented and the parameterisations used. Table S1 summarizes the main processes included in the GIMs used in the MME.

Masks

The analysis used here is not applicable when the runoff is very low. We therefore removed particularly arid areas from the analysis. We defined an arid cell to be one in which the time series from any emissions-climate-impact model combination (RCPs/GCMs/GIMs) had zero runoff for more than 90% of the time. Combining the arid cells from all RCPs/GCMs/GIMs combinations gave us a mask that removed 36% of the total land area from the analysis (32% of the JULES land area) (9 GIMs, Fig. S2 *Right*). Of the remaining cells, seasonal variation in total runoff led us to create a time-varying veto for each land cell and each RCPs/GCMs/GIMs combination, which discarded calendar days for which the value of Q90 was zero. For some GIMs, a significant number of points were vetoed at various times throughout the year (Fig. S3). To have sufficient coverage of the globe, we discarded the two GIMs (LPJmL and MATSIRO) for which the time-averaged number of vetoed points was greater than 25% for all climates. We then recalculated the mask with only the seven remaining GIMs (H08, JULES, Mac-PDM.09, MPI-HM, PCR-GLOBWB, VIC, and WBM). With this 7 GIMs mask, we remove 18% of the land cells from the analysis (17% of JULES land cells). See Fig. S2 *Left*.

Although we could not use LPJmL and MATSIRO data for analyzing global effects of the changing, we were able to use them to investigate the effect of CO_2 processes on the signal, by calculating subglobal GDIs using only the points available through the full 9 GIMs mask. This is therefore not a global investigation, but an investigation concentrating on the areas for which we had sufficient data for LPJmL and MATSIRO. Using HadGEM2-ES RCP8.5 runs, we demonstrate the effect on the sensitivity of the analysis to the inclusion of LPJmL and MATSIRO. The mean change is little affected by the addition of two GIMs, as it is 0.15 for the seven GIM analysis (Table S3) and 0.16 for nine GIMs. However, the S2N when using seven GIMs is 2.26 (Table S2). If we include all 9 GIMs, then the S2N decreases to 1.44. This decrease in sensitivity is probably because the 9 GIMs analysis considers a much smaller land surface area, due to vetoing of points in LPJmL and MATSIRO.

Effect of CO_2

Sensitivity tests were carried out with JULES and LPJmL to investigate the physiological and structural effect of increasing atmospheric CO_2 on the model. To exclude the effect of CO_2, runs were carried out in which the atmospheric CO_2 concentration provided as input to JULES and LPJmL was kept constant at a near present-day (i.e., year 2000) level throughout the 21st century. (Note that otherwise the GCM output used to force the model was identical to the standard run.) These sensitivity runs showed fundamentally different results regarding changes in global and regional drought frequency, with lower (higher) drought frequency simulated when the effect of CO_2 was included (excluded) (Fig. S5). A corresponding difference was seen in the vegetation, with a marked decrease in transpiration when CO_2 effects were included in both models, despite an increase in the carbon stored in vegetation (indicating an increase in vegetation biomass; Fig. S4 *Right*). Fig. S4 shows the difference in vegetation carbon and transpiration that can be associated with the inclusion of physiological and structural effects of CO_2 on the vegetation in JULES and LPJmL. The higher vegetation carbon seen when CO_2 increases to 2100 indicates more vigorous vegetation growth. Because the corresponding transpiration is lower, despite the increased vegetation, this decrease in transpiration can be associated with stomatal closure in a CO_2-rich atmosphere.

Fig. S5 demonstrates the sensitivity of JULES to representations of the effects of CO_2 on stomatal opening and dynamic vegetation. It shows the CDFs from HadGEM2-ES driven JULES runs where the CO_2 concentration was allowed to increase to 2100 ("CO_2") and where it was held constant at the 2000 value ("no CO_2"). For each CO_2 concentration, the vegetation was either dynamic, as in the standard JULES runs ("RCP8.5" in the legend), or fixed at a near-present day land use, LAI and height ("Fix. Veg."). Note that a single historical CDF is shown for clarity. With or without dynamic vegetation, the runs with constant CO_2 after year 2000 ("no CO_2") show a large increase in drought frequency under RCP8.5. With concentrations of CO_2 fixed, the stomata do not partially close as they do under higher CO_2, resulting in large evapotranspiration losses and increased drought. If we instead allow CO_2 to increase (and stomata to close) with fixed vegetation ("CO_2 Fix. Veg."), there is a smaller response because of reduced evaporative loss. Allowing both CO_2 and dynamic vegetation effects ("CO_2"), the stomata can close and conserve water; and now, where conditions become unfavorable, the vegetation will decline, and, where conditions are favorable, the vegetation will prosper. The net effect in these simulations from JULES is that there is little change in global drought in this case.

Regional Analysis

The regional analysis was conducted on a subset of 17 GEO subregions defined in ref. 1: North America (NAm); Meso America (MAm); Caribbean (Car); South America (SAm); Western Europe (WEu); Central Europe (CEu); Eastern Europe (EEu); Central Asia (CAs); East Asia and North West Pacific (EAs); South Asia (SAs); Southeast Asia (SEA); Australia and New Zealand (ANZ); Western Africa (WAf); Central Africa (CAf); Eastern Africa (EAf); Southern Africa (SAf); and Western Indian Ocean (WIO). The results for the regions and for global analysis are summarized in Table S3 (MME mean change) and Table S2 (Signal-to-Noise Ratio).

1. United Nations Environment Programme (2012) *GEO 5 Global Environment Oulook 5: Environment for the Future We Want* (United Nations Environment Programme, Nairobi, Kenya), p 551.

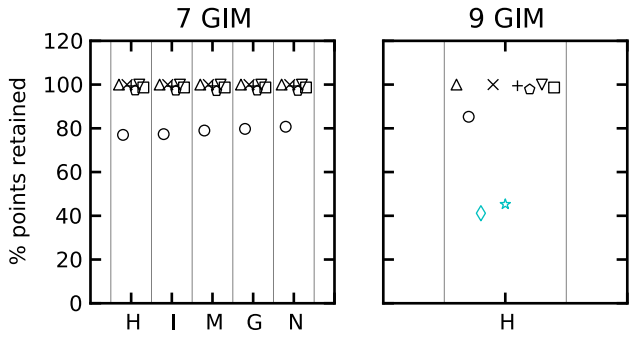

Fig. S1. The time-averaged fraction of unmasked land points used to calculate the GDI for mask calculated from 7 GIMS (*Left*) and mask calculated from 9 GIMS (*Right*) after vetoes were applied. The *x*-axis labels denote the different GCMs: H, HadGEM2-ES; I, IPSL-CM5A-LR; M, MIROC-ESM-CHEM; G, GFDL-ESM2M; and N, NorESM1-M. The 9 GIMs analysis was carried out using only HadGEM2-ES data. The colors indicate GIMs included in both 7 GIM and 9 GIM analyses (black), and GIMs included in only the 9 GIMs analysis (cyan). The symbols indicate the models: up triangle, H08; circle, JULES; x, Mac-PDM.09; +, MPI-HM; pentagon, PRCGLOB-WB; down triangle, VIC; square, WBM; diamond, LPJmL; star, MATSIRO.

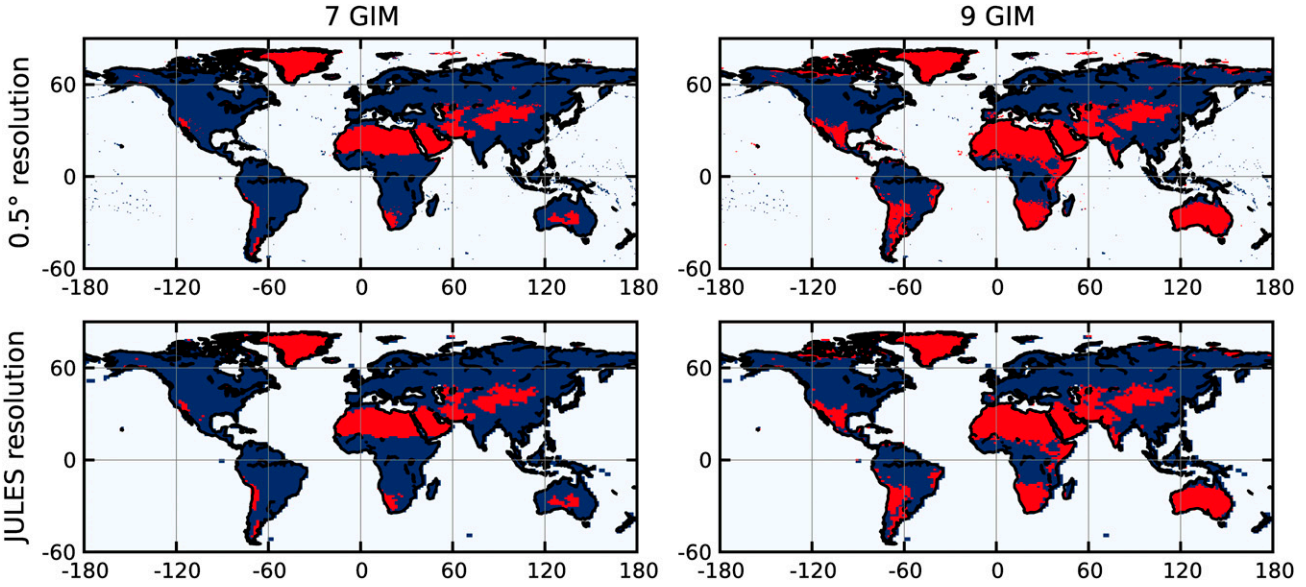

Fig. S2. Plot of the areas included in the analyses. Red areas were discarded whereas blue areas were retained. *Upper Left* shows the data included in the analysis of 7 GIMs for a 0.5° latitude × 0.5° longitude grid: 12,369 cells (18% of the total land area) were discarded; 55,051 cells (82% of the total land area) were retained. *Upper Right* shows the data included in the CO_2 sensitivity analysis for a 0.5° latitude × 0.5° longitude grid: 23,616 cells (36% of the total land area) were discarded; 43,804 cells (64% of the total land area) were retained (9 GIMs). *Lower Left* shows the data included in the analysis of 7 GIMs on the JULES grid: 1,288 cells (17% of the total land area) were discarded; 6,270 cells (83% of the total land area) were retained. *Lower Right* shows the data included in the CO_2 sensitivity analysis for the JULES grid: 2,356 cells (32% of the land area) were discarded; 5,202 cells (68% of the land area) were retained (9 GIMs).

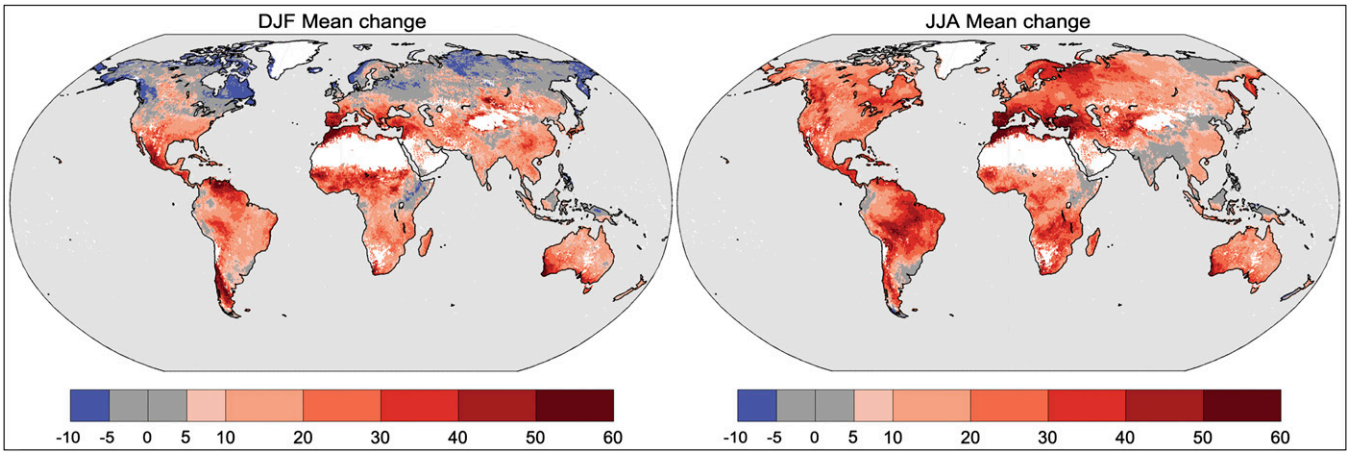

Fig. S3. Percentage change in the occurrence of days under drought conditions for two seasons for the period 2070–2099 relative to 1976–2005, based on a multimodel ensemble (MME) experiment under RCP8.5 from five global climate models and seven global impact models: MME mean change for December to February (DJF, *Left*) and June to August (JJA, *Right*). See *Methods* for definition of drought and masking procedure.

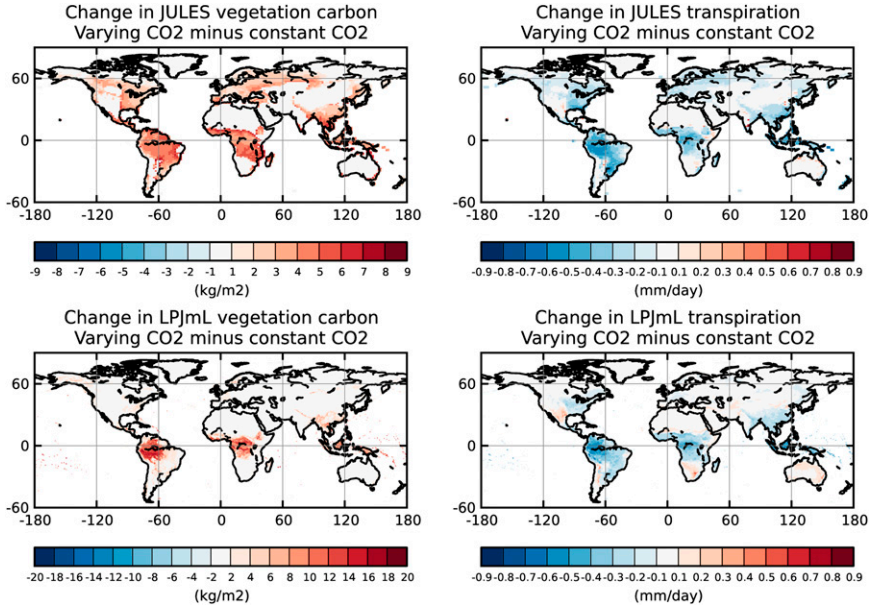

Fig. S4. Maps of the change in vegetation carbon and transpiration associated with the inclusion of effects of increased CO_2 on vegetation. These plots show the 2070–2099 average difference between the standard RCP8.5 HadGEM2-ES runs, with increasing CO_2 levels, and sensitivity runs where atmospheric CO_2 was held at a constant (year 2000) value throughout the 21st century. *Top Left* shows the change in JULES vegetation carbon associated with increasing CO_2 levels whereas *Top Right* shows the associated change in JULES transpiration. *Bottom Left* shows the change in vegetation carbon associated with increased CO_2 for LPJmL whereas *Bottom Right* shows the change in transpiration. A very similar pattern of increasing vegetation carbon coupled with a decrease in transpiration is seen in both models.

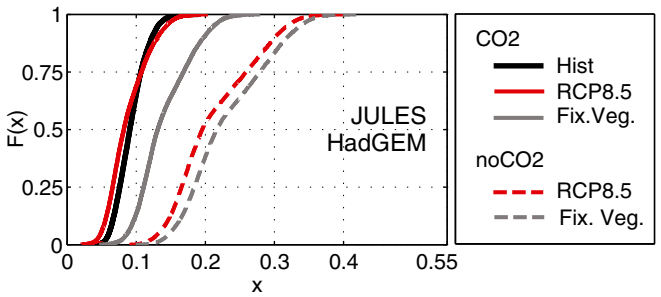

Fig. S5. Cumulative density functions of GDI for simulations of JULES using HadGEM2-ES forcing and showing the effects of different representations of CO_2 and vegetation dynamics. Colors show the representative concentration pathways: black, historical; red, RCP8.5. "CO2" and "no CO2" are runs with and without CO_2 increase after year 2000, with dynamic vegetation. "Fix. Veg. no CO2" and "Fix Veg. CO2" are runs with fixed vegetation, with and without variation of CO_2.

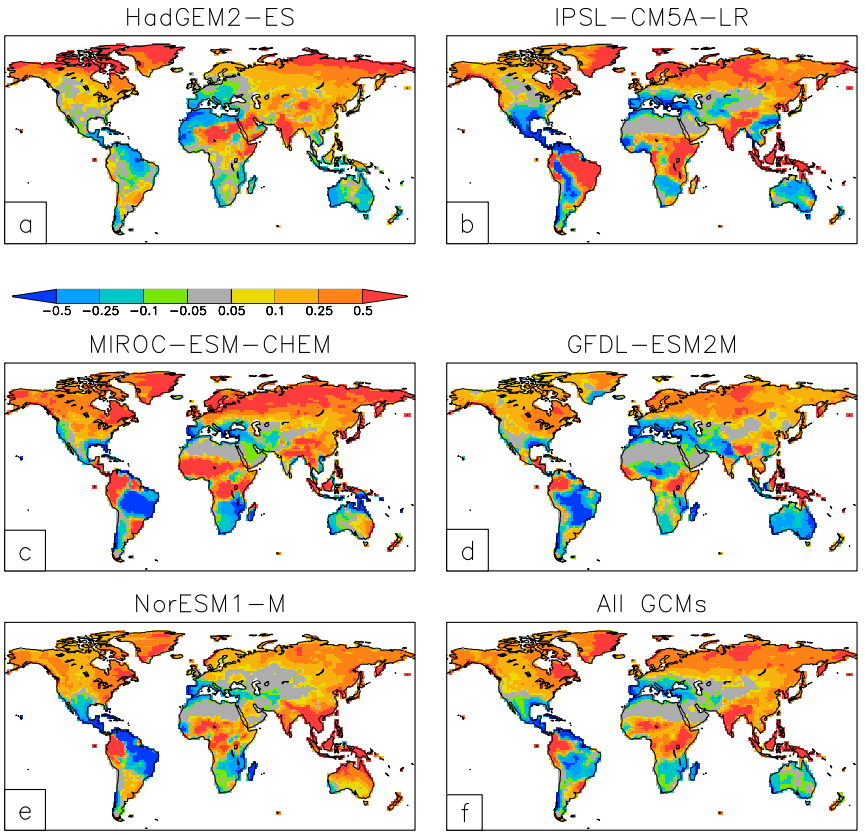

Fig. S6. Changes in mean annual precipitation between the reference (1976-2005) and future (2070-2099) time slices, expressed as a percentage of the reference amount, as simulated by HadGEM2-ES (*A*), IPSL-CM5A-LR (*B*), MIROC-ESM-CHEM (*C*), GFDL-ESM2M (*D*), and NorESM1-M (*E*), and the ensemble mean (*F*).

Table S1. Main characteristics of the Global Impact Models used in this study, after ref. 1

Model name	Time step length	Meteorological forcing*	Energy balance	Evaporation scheme†	Runoff scheme‡	Snow scheme	Vegetation dynamics	CO_2 effect§	Refs.
H08	Daily	R, S, T, W, Q, LW, SW, SP	Yes	Bulk formula	Saturation excess, nonlinear	Energy balance	No	No	(2)
JULES	30 min	R, S, T, W, Q, LW, SW, SP	Yes	Penman-Monteith (3)	Infiltration excess, saturation excess, groundwater.	Energy balance	Yes¶	Varying‖	(4, 5)
LPJmL	Daily	P, T, LW_n, SW	No	Priestley-Taylor (6)	Saturation excess	Degree-day	Yes	Varying‖	(7, 8)
MPI-HM	Daily	P, T, W, Q, LW, SW, SP	No	Penman-Monteith (3)	Saturation excess, nonlinear	Degree-day	No	No	(9, 10)
Mac-PDM.09	Daily	P, T, W, Q, LW_n, SW, SP	No	Penman-Monteith (3)	Saturation excess, nonlinear	Degree-day	No	No	(11, 12)
MATSIRO	1 h	R, S, T, W, Q, LW, SW, SP	Yes	Bulk formula	Infiltration excess, saturation excess, groundwater.	Energy balance	No	Constant (345 ppm)	(13)
PCRGlobWB	Daily	P, T	No	Hamon (14)	Infiltration excess, saturation excess, groundwater	Degree-day	No	No	(15–17)
VIC	Daily, 3 h snow	P, T_{max}, T_{min}, W, RH, LW, SW, SP.	Only for snow	Penman-Monteith (3)	Saturation excess, nonlinear	Energy balance.	No	No	(18)
WBM	Daily	P, T	No	Hamon (14)	Saturation excess	Empirical temp and precip based formula	No	No	(19–22)

*LW, downwelling longwave radiation; LW_n, net longwave radiation; P, precipitation rate (rain and snow calculated in the model); Q, air specific humidity; R, rainfall rate; RH, relative humidity; S, snowfall rate; SP, surface pressure; SW, downwelling shortwave radiation; T, air temperature; T_{max}, daily maximum air temperature; T_{min}, daily minimum air temperature; W, wind speed.
†Bulk formula: Bulk transfer coefficients are used when calculating turbulent heat fluxes.
‡Nonlinear: Subsurface runoff is a nonlinear function of soil moisture.
§CO_2 concentration in calculation of stomatal conductance.
¶Vegetation dynamics were switched off in sensitivity experiments.
‖CO_2 variation was switched off in sensitivity experiments.

1. Haddeland I, et al. (2011) Multimodel Estimate of the Global Terrestrial Water Balance: Setup and First Results. *Journal of Hydrometeorology* 12(5):869–884.
2. Hanasaki N, et al. (2008) An integrated model for the assessment of global water resources – Part 1: Model description and input meteorological forcing. *Hydrol Earth Syst Sci* 12(4): 1007–1025.
3. Allen RG, Pereira LS, Raes D, Smith M (1998) FAO irrigation and drainage paper 56 - Crop evapotranspiration - Guidelines for computing crop water requirements. (Food and Agriculture Organisation of the United Nations, Rome), p 300.
4. Clark DB, et al. (2011) The Joint UK Land Environment Simulator (JULES), model description – Part 2: Carbon fluxes and vegetation dynamics. *Geosci Model Dev* 4(3):701–722.
5. Best MJ, et al. (2011) The Joint UK Land Environment Simulator (JULES), model description – Part 1: Energy and water fluxes. *Geosci Model Dev* 4(3):677–699.
6. Priestley CHB, Taylor RJ (1972) On the assessment of surface heat flux and evaporation using large-scale parameters. *Monthly Weather Review* 100(2):81–92.
7. Bondeau A, et al. (2007) Modelling the role of agriculture for the 20th century global terrestrial carbon balance. *Global change biology* 13(3):679-706.
8. Rost S, et al. (2008) Agricultural green and blue water consumption and its influence on the global water system. *Water Resources Research* 44(9):W09405.
9. Hagemann S, Gates LD (2003) Improving a subgrid runoff parameterization scheme for climate models by the use of high resolution data derived from satellite observations. *Climate Dynamics* 21:349–359.
10. Stacke T, Hagemann S (2012) Development and evaluation of a global dynamical wetlands extent scheme. *Hydrol Earth Syst Sci* 16(8):2915–2933.
11. Gosling SN, Arnell NW (2011) Simulating current global river runoff with a global hydrological model: model revisions, validation, and sensitivity analysis. *Hydrological Processes* 25:1129–1145.
12. Arnell NW (1999) A simple water balance model for the simulation of streamflow over a large geographic domain. *Journal of Hydrology* 217(3–4):314–335.
13. Takata K, Emori S, Watanabe T (2003) Development of the minimal advanced treatments of surface interaction and runoff. *Global and Planetary Change* 38(1–2):209–222.
14. Hamon WR (1961) Estimating potential evapotranspiration. *Journal of the Hydraulics Division - Proceedings of the American Society of Civil Engineers* 87(HY3):107–120.
15. Wada Y, et al. (2011) Global monthly water stress: 2. Water demand and severity of water stress. *Water Resources Research* 47(7):W07518.
16. Wada Y, et al. (2010) Global depletion of groundwater resources. *Geophysical Research Letters* 37(20):L20402.
17. van Beek LPH, Wada Y, Bierkens MFP (2011) Global monthly water stress: 1. Water balance and water availability. *Water Resources Research* 47(7):W07517.
18. Liang X, Lettenmaier DP, Wood EF, Burges SJ (1994) A simple hydrologically based model of land surface water and energy fluxes for general circulation models. *Journal of Geophysical Research: Atmospheres* 99(D7):14415–14428.
19. Vörösmarty CJ, et al. (1989) Continental scale models of water balance and fluvial transport: An application to South America. *Global Biogeochemical Cycles* 3(3):241–265.
20. Vörösmarty CJ, Federer CA, Schloss AL (1998) Potential evaporation functions compared on US watersheds: Possible implications for global-scale water balance and terrestrial ecosystem modeling. *Journal of Hydrology* 207(3–4):147–169.
21. Wisser D, et al. (2008) Global irrigation water demand: Variability and uncertainties arising from agricultural and climate data sets. *Geophysical Research Letters* 35(24):L24408.
22. Wisser D, Fekete BM, Vörösmarty CJ, Schumann AH (2010) Reconstructing 20th century global hydrography: a contribution to the Global Terrestrial Network- Hydrology (GTN-H). *Hydrol Earth Syst Sci* 14(1):1–24.
23. UNEP (2012) GEO 5 Global Environment Oulook 5 - Environment for the future we want. p 551.

Table S2. Ensemble signal-to-noise ratio (ensemble mean change divided by its inter-quartile range IQ) associated with changes in global and regional deficit indices

				RCP8.5														
	RCP2.6	RCP4.5	RCP6.0		Uncertainty in GIMs						Uncertainty in GCMs							
Regional extent	All GCMs & GIMs	All GCMs & GIMs	All GCMs & GIMs	All GCMs & GIMs (6GIMs)	HadGEM2-ES all GIMs (6GIMs)	IPSL-CM5A-LR all GIMs (6GIMs)	MIROC-ESM-CHEM all GIMs (6GIMs)	GFDL-ESM2M all GIMs (6GIMs)	NorESM1-M all GIMs (6GIMs)	Average all GIMs (6GIMs)	H08 all GCMs	JULES all GCMs	Mac-PDM.09 all GCMs	MPI-HM all GCMs	PCRGlobWB all GCMs	VIC all GCMs	WBM all GCMs	GCMs Average all GIMs (6GIMs)
Globe S2N: mean/SD	1.35	1.23	1.26	1.67 (3.24)	1.94 (4.57)	1.91 (4.56)	1.63 (3.84)	1.27 (3.36)	1.69 (4.18)	1.69 (4.10)	3.38	−1.44	4.33	4.13	5.30	3.94	3.49	3.30 (4.10)
Globe S2N: mean/IQ	1.18	0.89	1.13	1.44 (2.40)	1.92 (2.89)	2.14 (3.02)	1.92 (2.48)	1.46 (1.92)	1.68 (2.08)	1.82 (2.48)	2.22	−0.97	3.91	2.78	3.71	2.99	2.42	2.44 (3.01)
North America (NAm)	0.33	0.44	0.65	0.70 (1.51)	1.96 (2.58)	1.38 (2.05)	1.18 (1.83)	0.57 (1.28)	1.45 (2.00)	1.31 (1.95)	1.68	−1.80	1.40	1.69	1.77	1.27	1.29	1.04 (1.52)
Meso-America (MAm)	0.47	0.76	0.78	0.80 (0.93)	1.99 (2.69)	3.22 (3.76)	1.57 (2.59)	1.19 (0.38)	2.64 (3.13)	2.12 (2.51)	0.90	0.28	0.72	0.88	0.90	0.74	0.79	0.74 (0.82)
Caribbean (Car)	0.19	0.57	0.72	0.80 (0.87)	1.96 (2.34)	1.55 (2.04)	0.82 (1.12)	0.23 (0.97)	2.52 (3.18)	1.42 (1.93)	0.70	0.15	0.65	0.85	0.88	0.75	0.92	0.70 (0.79)
South America (SAm)	1.16	1.32	1.48	1.52 (2.66)	4.29 (6.16)	1.61 (1.91)	2.42 (2.87)	0.94 (1.17)	2.40 (2.77)	2.33 (2.98)	3.32	0.35	1.57	5.81	2.01	1.87	1.47	2.34 (2.68)
Western Europe (WEu)	1.06	0.99	1.53	1.69 (2.27)	1.81 (2.19)	2.25 (2.78)	2.22 (2.94)	2.01 (2.52)	2.06 (2.39)	2.07 (2.56)	5.93	0.63	6.59	4.88	2.57	4.47	7.55	4.66 (5.33)
Central Europe (CEu)	0.81	089	1.10	1.55 (1.75)	7.79 (2.34)	3.19 (4.58)	3.19 (3.78)	6.17 (9.73)	1.91 (2.90)	4.45 (4.67)	1.80	0.30	1.19	2.34	1.29	1.64	0.97	1.36 (1.54)
Eastern Europe (EEu)	−0.15	0.11	0.20	0.55 (1.10)	1.75 (2.56)	1.57 (2.70)	0.51 (0.94)	−0.42 (0.17)	1.77 (3.23)	1.04 (1.92)	0.81	−2.66	1.25	1.17	1.52	1.51	2.01	0.80 (1.38)
Central Asia (CAs)	0.36	0.41	0.48	0.71 (0.84)	0.52 (0.90)	1.73 (3.11)	1.23 (4.93)	1.29 (2.98)	1.22 (2.05)	1.20 (2.79)	0.85	−0.25	1.18	0.74	0.65	0.69	0.72	0.65 (0.81)
East Asia (EAs)	0.97	0.79	1.11	1.32 (1.80)	1.10 (1.31)	1.29 (1.52)	1.36 (1.62)	1.54 (2.00)	1.22 (1.87)	1.30 (1.66)	0.99	−0.11	1.23	1.13	1.23	1.43	1.21	1.02 (1.20)
South Asia (SAs)	0.48	0.40	0.44	0.59 (0.95)	0.23 (0.59)	0.72 (1.11)	0.97 (1.35)	1.37 (2.33)	0.56 (0.82)	0.77 (1.24)	1.51	−0.67	0.54	1.38	0.87	0.68	0.49	0.69 (0.91)
South East Asia (SEA)	0.77	0.47	0.51	0.47 (0.64)	1.51 (1.94)	0.88 (1.18)	0.60 (0.79)	0.30 (0.74)	−0.36 (-0.26)	0.59 (0.88)	0.50	−0.84	0.25	0.56	0.67	0.31	0.43	0.27 (0.45)
Australia and New Zealand (ANZ)	1.15	1.01	0.77	0.91 (1.45)	1.42 (0.90)	2.35 (3.11)	1.86 (4.93)	1.21 (2.98)	0.33 (2.05)	1.43 (2.79)	2.20	0.07	2.46	2.00	5.88	2.18	1.40	2.31 (2.69)
Western Africa (WAf)	0.33	0.49	0.51	0.73 (0.91)	1.23 (2.76)	1.92 (3.17)	0.10 (0.31)	0.91 (2.12)	0.64 (0.84)	0.96 (1.84)	0.54	−0.08	0.48	0.63	0.98	0.55	0.56	0.52 (0.62)
Central Africa (CAf)	1.23	0.94	0.87	0.84 (1.42)	1.82 (2.57)	1.75 (2.67)	0.46 (0.65)	1.20 (1.55)	1.77 (9.35)	1.40 (3.36)	1.09	−0.66	0.80	1.04	2.75	2.18	1.70	1.27 (1.59)
Eastern Africa (EAf)	0.11	0.15	0.04	0.00 (0.15)	0.41 (0.60)	−1.26 (-1.32)	−0.05 (0.14)	−0.49 (-0.43)	0.25 (0.87)	−0.23 (-0.03)	0.26	−2.87	−0.04	−0.03	0.66	−0.79	0.02	−0.40 (0.01)
Southern Africa (SAf)	0.98	0.84	0.84	1.07 (1.39)	1.06 (1.34)	0.92 (1.14)	1.18 (1.56)	0.73 (0.99)	1.15 (1.43)	1.01 (1.29)	2.41	−0.49	1.14	2.32	1.81	1.63	1.00	1.40 (1.72)
Western Indian Ocean (WIO)	1.13	1.19	1.09	1.27 (1.47)	1.02 (1.83)	0.43 (0.56)	0.93 (1.11)	1.35 (2.03)	1.31 (1.85)	1.01 (1.48)	1.59	0.12	2.24	3.17	2.12	3.57	1.11	1.99 (2.30)

Multimodel experiment as in Table S3. Regions are the GEO subregions of ref. 1.

1. United Nations Environment Programme (2012) *GEO 5 Global Environment Oulook 5: Environment for the Future We Want* (United Nations Environment Programme, Nairobi, Kenya), p 551.

Table S3. Ensemble mean changes in global and regional deficit indices under different RCPs from a multimodel experiment using seven global impact models driven by five CMIP5 global climate models considering all members together or subset of members

	RCP2.6	RCP4.5	RCP6.0	RCP8.5												
Regional extent	All GCMs & GIMs	All GCMs & GIMs	All GCMs & GIMs	All GCMs & GIMs (6GIMs)	HadGEM2-ES all GIMs (6GIMs)	IPSL-CM5A-LR all GIMs (6GIMs)	MIROC-ESM-CHEM all GIMs (6GIMs)	GFDL-ESM2M all GIMs (6GIMs)	NorESM1-M all GIMs (6GIMs)	H08 all GCMs	JULES all GCMs	Mac-PDM.09 all GCMs	MPI-HM all GCMs	PCRGlobWB all GCMs	VIC all GCMs	WBM all GCMs
Globe	0.039	0.063	0.074	0.130 (0.156)	0.153 (0.180)	0.163 (0.192)	0.133 (0.161)	0.078 (0.099)	0.122 (0.147)	0.135	−0.024	0.115	0.193	0.202	0.157	0.133
Globe (IQ range)	*0.033*	*0.071*	*0.065*	*0.090 (0.065)*	*0.080 (0.062)*	*0.076 (0.063)*	*0.069 (0.065)*	*0.053 (0.051)*	*0.073 (0.071)*	*0.061*	*0.025*	*0.029*	*0.069*	*0.054*	*0.052*	*0.055*
North America (NAm)	0.008	0.032	0.040	0.088 (0.113)	0.081 (0.106)	0.149 (0.180)	0.103 (0.132)	0.015 (0.029)	0.092 (0.118)	0.074	−0.062	0.083	0.115	0.153	0.148	0.107
Meso-America (MAm)	0.038	0.123	0.123	0.247 (0.276)	0.253 (0.274)	0.441 (0.486)	0.123 (0.154)	0.015 (0.029)	0.402 (0.437)	0.260	0.072	0.220	0.377	0.332	0.224	0.242
Caribbean (Car)	0.010	0.115	0.108	0.216 (0.245)	0.304 (0.335)	0.265 (0.297)	0.093 (0.124)	0.020 (0.039)	0.396 (0.428)	0.173	0.043	0.178	0.373	0.290	0.186	0.269
South America (SAm)	0.086	0.125	0.140	0.216 (0.247)	0.289 (0.324)	0.183 (0.213)	0.257 (0.293)	0.127 (0.154)	0.223 (0.253)	0.240	0.026	0.192	0.292	0.337	0.197	0.227
Western Europe (WEu)	0.044	0.100	0.126	0.208 (0.238)	0.247 (0.277)	0.230 (0.263)	0.205 (0.236)	0.128 (0.150)	0.232 (0.264)	0.187	0.030	0.181	0.280	0.277	0.302	0.202
Central Europe (CEu)	0.070	0.130	0.148	0.282 (0.317)	0.252 (0.283)	0.440 (0.474)	0.317 (0.359)	0.178 (0.207)	0.221 (0.261)	0.278	0.070	0.259	0.385	0.321	0.352	0.308
Eastern Europe (EEu)	−0.005	0.007	0.015	0.057 (0.077)	0.085 (0.108)	0.075 (0.097)	0.048 (0.069)	−0.009 (0.002)	0.084 (0.107)	0.044	−0.064	0.048	0.073	0.076	0.138	0.081
Central Asia (CAs)	0.020	0.034	0.068	0.108 (0.132)	0.039 (0.061)	0.200 (0.223)	0.100 (0.124)	0.016 (0.032)	0.184 (0.218)	0.098	−0.035	0.144	0.208	0.120	0.136	0.084
East Asia (EAs)	0.038	0.045	0.075	0.110 (0.130)	0.097 (0.115)	0.188 (0.213)	0.101 (0.119)	0.080 (0.097)	0.084 (0.104)	0.128	−0.007	0.084	0.168	0.142	0.177	0.079
South Asia (SAs)	0.030	0.032	0.062	0.083 (0.104)	0.010 (0.022)	0.092 (0.115)	0.100 (0.127)	0.159 (0.184)	0.054 (0.075)	0.124	−0.046	0.067	0.150	0.143	0.077	0.066
South East Asia (SEA)	0.024	0.031	0.036	0.061 (0.079)	0.162 (0.190)	0.071 (0.089)	0.074 (0.097)	0.013 (0.027)	−0.017 (-0.008)	0.077	−0.050	0.035	0.109	0.155	0.035	0064
Australia and New Zealand (ANZ)	0.084	0.079	0.089	0.152 (0.175)	0.192 (0.215)	0.194 (0.225)	0.187 (0.204)	0.164 (0.197)	0.020 (0.037)	0.141	0.008	0.179	0.263	0.191	0.171	0.107
Western Africa (WAf)	0.035	0.063	0.072	0.158 (0.186)	0.181 (0.213)	0.349 (0.395)	0.008 (0.020)	0.175 (0.205)	0.079 (0.099)	0.167	−0.010	0.133	0.285	0.242	0.117	0.175
Central Africa (CAf)	0.085	0.119	0.116	0.158 (0.188)	0.190 (0.225)	0.234 (0.273)	0.077 (0.099)	0.176 (0.205)	0.115 (0.136)	0.139	−0.018	0.112	0.170	0.356	0.125	0.225
Eastern Africa (EAf)	0.008	0.017	0.003	0.000 (0.012)	0.051 (0.068)	−0.046 (-0.042)	−0.004 (0.007)	−0.018 (-0.008)	0.019 (0.033)	0.032	−0.066	−0.003	−0.003	0.081	−0.040	0.001
Southern Africa (SAf)	0.079	0.122	0.106	0.198 (0.236)	0.229 (0.268)	0.147 (0.180)	0.264 (0.312)	0.131 (0.162)	0.220 (0.256)	0.258	−0.027	0.132	0.367	0.309	0.207	0.140
Western Indian Ocean (WIO)	0.096	0.139	0.151	0.197 (0.228)	0.247 (0.279)	0.086 (0.110)	0.198 (0.234)	0.261 (0.296)	0.194 (0.223)	0.202	0.009	0.111	0.319	0.399	0.187	0.153

Regions are the GEO subregions of ref. 1. Second row (italic) gives the Inter-Quartile (IQ) range of Global Deficit Index MME changes.

1. United Nations Environment Programme (2012) *GEO 5 Global Environment Oulook 5: Environment for the Future We Want* (United Nations Environment Programme, Nairobi, Kenya), p 551.